

RESEARCH ARTICLE | SEPTEMBER 10 2024

Influence of the inner roughness of powder channels on the powder propagation behavior in laser metal deposition ^{EP}

Special Collection: [Proceedings of the International Congress of Applications of Lasers & Electro-Optics \(ICALEO 2024\)](#)

Annika Bohlen ^{ID} ; Thomas Seefeld ^{ID}

 Check for updates

J. Laser Appl. 36, 042007 (2024)

<https://doi.org/10.2351/7.0001570>



Articles You May Be Interested In

Characterization of the powder stream propagation behavior of a discrete coaxial nozzle for laser metal deposition

J. Laser Appl. (November 2022)

Powder catchment efficiency in laser cladding (directed energy deposition). An investigation into standard laser cladding and the ABA cladding technique

J. Laser Appl. (February 2023)

Adaptive powder nozzle setup for enhanced efficiency in laser metal deposition

J. Laser Appl. (January 2024)



Influence of the inner roughness of powder channels on the powder propagation behavior in laser metal deposition

Cite as: J. Laser Appl. 36, 042007 (2024); doi: 10.2351/7.0001570

Submitted: 29 June 2024 · Accepted: 12 August 2024 ·

Published Online: 10 September 2024



Annika Bohlen¹  and Thomas Seefeld^{1,2} 

AFFILIATIONS

¹BIAS—Bremer Institut für angewandte Strahltechnik GmbH, Klagenfurter Str. 5, Bremen 28359, Germany

²MAPEX Center for Materials and Processes, Universität Bremen, Bibliothekstraße 1, Bremen 28359, Germany

Note: Paper published as part of the special topic on Proceedings of the International Congress of Applications of Lasers & Electro-Optics 2024.

ABSTRACT

The powder propagation behavior of powder nozzles for the laser metal deposition process has a significant influence on powder utilization rate and track geometry. A well-focused powder stream will lead to a higher process efficiency and lower material loss. Powder channels with different roughness and a constant diameter of 1.5 mm were placed by wire electrical discharge machining into a copper alloy printed by powder bed fusion. Nickel base powder with a size of -106 to $+45\ \mu\text{m}$ was delivered through the powder channels with varied carrier gas flow rates and varied powder mass flow rates. High-speed imaging was used to analyze the powder flow. From these recordings, the dispersion angle of the powder stream from single channels could be measured as well as the velocity of particles. Moreover, the relationship between individual particle velocity and individual particle flight angle was investigated. It was found that the inner roughness of powder channels has a major impact on powder propagation behavior. It could be shown that with a decrease in R_a from 2.16 to $0.27\ \mu\text{m}$ the divergence angle decreased by around 61% while the particle velocity was increased by at least 28% for all varied parameters. Particles with a high velocity tend to have a lower particle flight angle.

Key words: laser metal deposition, powder stream propagation, particle velocity, powder stream divergence, surface roughness angle, high-speed imaging

© 2024 Author(s). All article content, except where otherwise noted, is licensed under a Creative Commons Attribution (CC BY) license (<https://creativecommons.org/licenses/by/4.0/>). <https://doi.org/10.2351/7.0001570>

I. INTRODUCTION

Laser metal deposition (LMD) has become an increasingly important process in recent decades.¹ In addition to the production of 3D-printed components, other important areas of application include the repair of high-quality components. In order to ensure economic efficiency, it is essential to consider both process efficiency and resource efficiency. The design of the powder feed is of great importance in both of these areas. In terms of resource efficiency, it is important that the powder utilization rate is as high as possible, as this minimizes the wastage of raw materials. At the same time, a high powder utilization rate also allows for a high buildup rate. A powder nozzle should also have the largest possible working distance and a large working area. The large working

distance often protects the sensitive powder nozzle from heat generated by the process and from flying powder particles that can stick to it. The expansive working area enables the process to remain stable, even in the event of minor discrepancies in the distance between the workpiece and nozzle. It is crucial to maintain a narrow divergence angle of the powder stream to ensure a substantial working distance with a broad working range and precise focusing of the powder stream simultaneously. It is imperative that both of these aspects be met in order to guarantee the uninterrupted production of components or repairs.

Particle-wall collisions are known to have an impact on both divergence angle and particle velocity.² A real collision between two bodies leads to a reduction in velocity, as this impact is a mixture of elastic and plastic impact. The key figure to describe this

26 March 2025 14:09:59

relationship is the coefficient of restitution (COR). This results from the ratio of the velocities of the two bodies before and after the impact v_1/v_2 . The studies by Odum *et al.* concentrate on the experimental determination of the normal COR. The velocities before and after an impact of 316L powder with a size distribution of 45–105 μm were investigated. Different materials with different roughnesses were selected as counterparts. The impact velocities were in the typical LMD range, between 0.65 and 13.55 m/s. The roughness of the substrates ranged from approximately $Ra=0.1$ to $Ra=0.7\ \mu\text{m}$. The observed normal components of the COR values exhibited a range of 0.42–0.55. The normal COR was influenced by the material of the counter body, the speed before the impact, and the impact angle. However, the authors did not observe an influence of surface roughness on the normal COR.³

In addition to the influence on the particle velocity, particle-wall collisions also have an influence on the divergence angle of the emerging powder. The experimental and numerical investigations of powder nozzles by Polyanskiy *et al.* demonstrated that the divergence angle for copper injectors is between 10° and 11°, while it reaches a value between 30° and 35° for steel injectors. This phenomenon can be attributed to the differing scattering of rebound angles for different materials, which the particle trajectories undergo following their exit from the nozzle.⁴

In their investigation of the influence of roughness in single injectors for the LMD process, Jeromen *et al.* employed numerical calculations and experiments. They utilized the standard deviation of the surface roughness angle $\sigma\gamma$, defined as the angle between the collision normal of a particle and the normal of the centerline of the surface roughness profile (see Fig. 1), as a metric to characterize the impact of surface roughness on particle-wall collisions.⁵ This approach was inspired by Sommerfeld,⁶ who proposed this specific measure of surface roughness. A spherical particle with a diameter of d_p was assumed for the definition of the surface roughness angle. Following Sommerfeld and Huber,⁷ the distribution of the surface roughness angle γ can be described as normal, with a mean value of zero and a selected standard deviation $\sigma\gamma$. The calculation

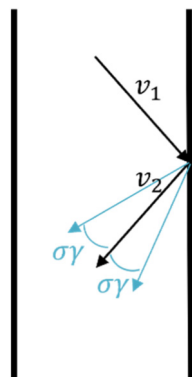


FIG. 1. Schematic illustrating the standard deviation of the surface roughness angle $\sigma\gamma$.

is performed according to the following equation:⁸

$$\sigma\gamma = \begin{cases} \arctan\left(\frac{Ra}{2 \cdot RSm}\right); & d_p > RSm, \\ \arctan\left(\frac{2 \cdot Ra}{RSm}\right); & d_p < RSm. \end{cases} \quad (1)$$

Previous numerical simulations of powder flow have demonstrated that wall roughness plays a significant role in achieving a powder flow with minimal divergence. Additionally, it has been demonstrated that an increase in the value of $\sigma\gamma$ results in a reduction in particle velocity.⁹

This paper examines the impact of varying inner powder channel roughnesses and the resulting standard deviation of the surface roughness angle ($\sigma\gamma$) on the divergence of powder stream and particle velocities. To this end, a powder bed-printed HOVADUR CNCS cuboid with powder channels of varying inner surface roughnesses was employed. The powder stream from each channel was observed by a high-speed camera and subjected to comprehensive analysis.

II. EXPERIMENTAL SETUP AND METHODS

A. Materials

The powder material was a nickel base alloy (EuTroloy 16625G.04) with a nominal particle size of -106 to $+45\ \mu\text{m}$, sourced from Castolin Eutectic Ireland Ltd. The chemical composition of the powder material is presented in Table I. The scanning electron microscope (SEM) images (Fig. 2) of the powder demonstrate that the powder particles are primarily spherical, with satellite particles. A few particles exhibit an irregular shape.

A cuboid of HOVADUR CNCS was printed with powder bed fusion by the company Schmelzmetall. The chemical composition can be found in Table II. Subsequently, powder channels were placed into the cuboids by wire electrical discharge machining (by the Institute for Machine Tools and Factory Management, Technische Universität Berlin), resulting in the production of five channels with varying surface roughness. The channels were circular in shape, with a diameter of $1.54 \pm 0.04\ \text{mm}$. The length of the powder channel is 19 mm (see Fig. 3) after placement of thread.

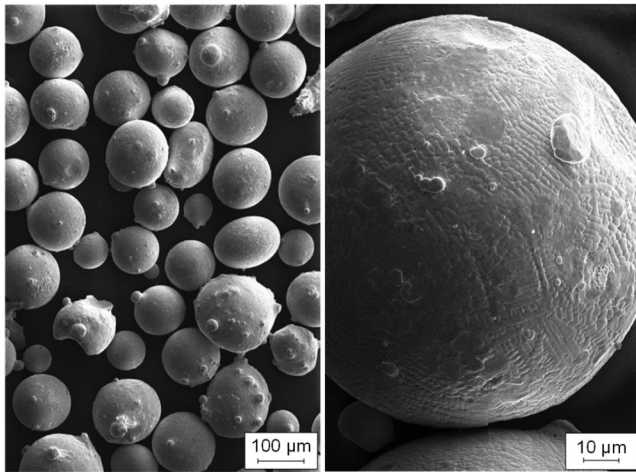
B. Inner channel surface roughness measurement

Following the completion of the experiments, the channels were cut in half by electrical discharge machining in order to

TABLE I. Chemical composition in % of weight of EuTroloy powder.

	%		%	
Al	0.01	N	0.11	
C	0.01	Nb	3.57	
Si	0.43	Ti	0.01	
Fe	0.40	O	0.070	
Mn	0.38	Cr	21.20	
Mo	8.90	Ni	Bal.	

26 March 2025 14:09:59



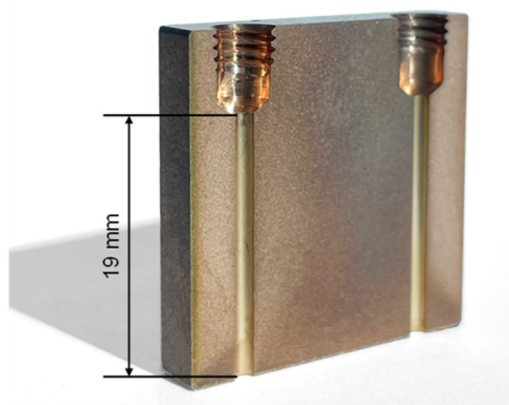
Bohlen 2024

BIAS ID 240230

FIG. 2. SEM images of the powder.

TABLE II. Chemical composition in % of weight of HOVADUR CNCS.

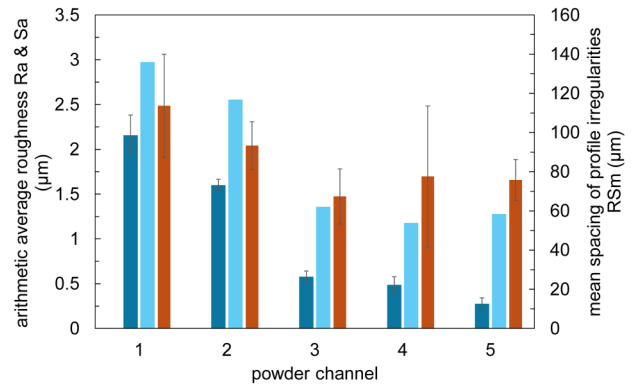
%		%	
Ni	2.0–3.0	Mn	Max. 0.1
Si	0.5–0.8	Pb	Max. 0.02
Cr	0.2–0.5	Other metals	Max. 0.1
Fe	Max. 0.15	Cu	Bal.



Bohlen 2024

BIAS ID 240231

FIG. 3. Powder bed fusion printed specimen of HOVADUR with powder channels placed by wire electrical discharge machining, cut in half by electrical discharge machining.



Confocal microscope: Keyence VKX 3000
Magnification: 50x
 λ_s/S -Filter: 0.8 μm
 λ_c/L -Filter: 0.8 mm

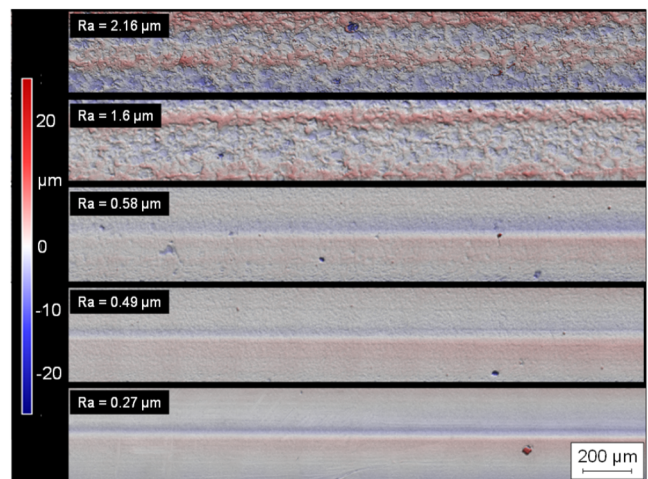
Bohlen 2024

BIAS ID 240232

FIG. 4. Arithmetic average roughness values Ra and Sa and mean spacing of profile irregularities RSm for all five powder channels.

measure their roughness. To measure the roughness, a Keyence VK 9700 confocal microscope was utilized with a 50 \times magnification and a numerical aperture (NA) of 0.55. Several images were combined to achieve a measurement length of at least 4 mm. Following the correction of the surface shape in order to flatten the curved data, the measurement data were filtered with a low-pass (λ_s) filter of 0.8 μm and a high-pass (λ_c) filter of 0.8 mm. The roughness profiles were then extracted using 10 parallel lines with a distance of 13.9 μm , and the values Ra and RSm were determined using these. The surface arithmetic average roughness Sa was also measured

26 March 2025 14:09:59



Bohlen 2024

BIAS ID 240233

FIG. 5. Topography of the powder channels with five different surface roughness values.

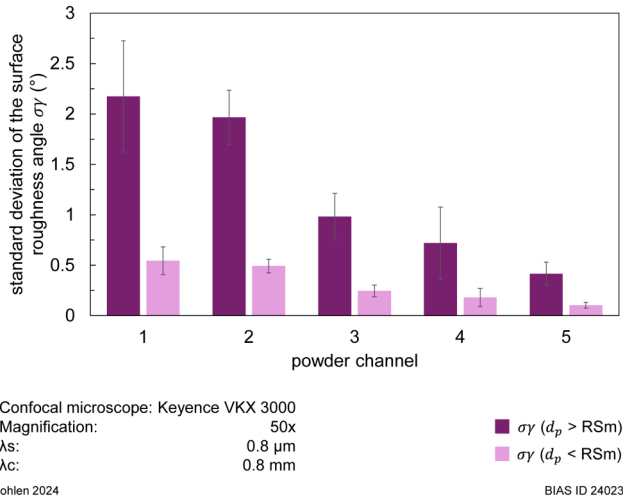


FIG. 6. Calculated standard deviations of the surface roughness angle σ_γ for both cases $d_p > RSm$ and $d_p < RSm$.

using the same values for low-pass and high-pass filters as for the line roughness. The diagram in Fig. 4 shows all measured values.

Figure 5 depicts a representative excerpt from the measurement topography of the five inner channel surfaces. The presence of defects within the surface can be observed in instances where a smoother finish is present. These defects are likely the result of imperfections in the HOVADUR CNCS samples, such as pores and bonding defects, which are inherent to the powder bed process.

The standard deviations of the surface roughness angle σ_γ for both cases described in Formula (1) were calculated (Fig. 6).

C. Carrier gas velocity measurement

The velocity of the carrier gas was quantified using a Prandtl tube. The tube was positioned 10 mm beneath the channel exit,

oriented directly into the gas stream. Each measurement was repeated five times.

D. High-speed imaging and analysis

High-speed videos were captured using an i-Speed 7 high-speed camera from iX Cameras. All videos were captured at a frame rate of 45 kHz to observe the particles ejected from the powder channel and had a minimum resolution of 21 $\mu\text{m}/\text{px}$. The videos were illuminated using a Cavilux illumination laser from Cavitar. Particle tracking was conducted with TrackMate¹⁰ within IMAGEJ software.

The high contrast achieved in the videos through the use of the illumination laser enabled automated particle detection after background reduction. Particles were tracked and information on each detection was saved. From these, individual trajectories could be calculated, including the mean velocity within each particle track and their flight angle. Rebounding particles (having a negative velocity) were filtered from the results. The mean particle velocity $\pm 2\sigma$ and their corresponding particle flight angles were divided into bins (according to the Freedman–Diaconis rule). For each of these bins, the 2σ of the particle flight angles was calculated.

To calculate the divergence angle of the powder, a background model of the video was first calculated from all 10 000 frames. The background model was then subtracted from each individual frame, and the resulting binary images were summed up to create an intensity map of the particles' locations over 10 000 frames (see Fig. 7). The intensity along a line, orthogonal to the powder channel, situated close to the channel exit and at a distance of approximately 15 mm to the channel exit, was extracted. A Gaussian fit was calculated for this intensity, with 2σ marking the boundary of the powder stream. The divergence angle was then calculated between these boundaries.

III. RESULTS

Particle velocities as a function of increasing powder mass flow rate for different inner channel roughness values are presented in Fig. 8. It can be observed that with increasing powder mass flow

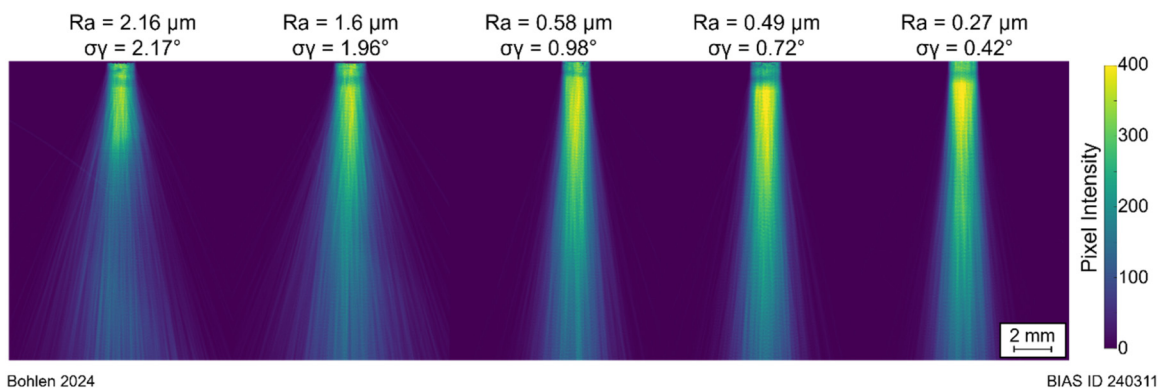
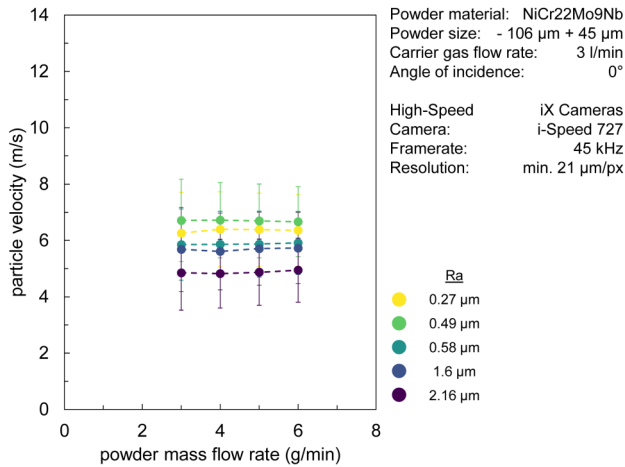


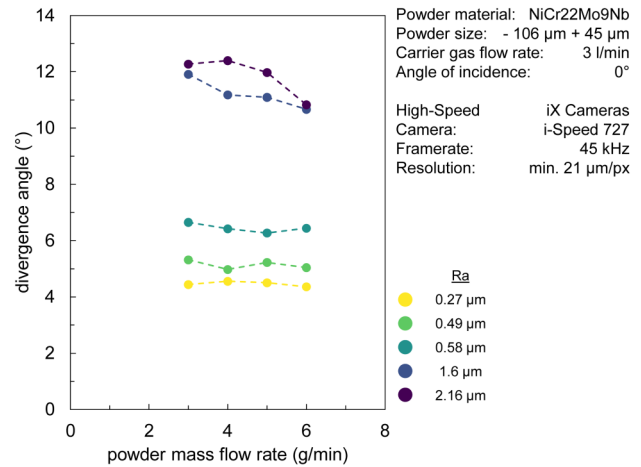
FIG. 7. Intensity map of the particles' locations over 10 000 frames for different inner channel roughness Ra.

26 March 2025 14:09:59



Bohlen 2024 BIAS ID 240235

FIG. 8. Particle velocity as a function of the powder mass flow rate for different inner channel roughness Ra.

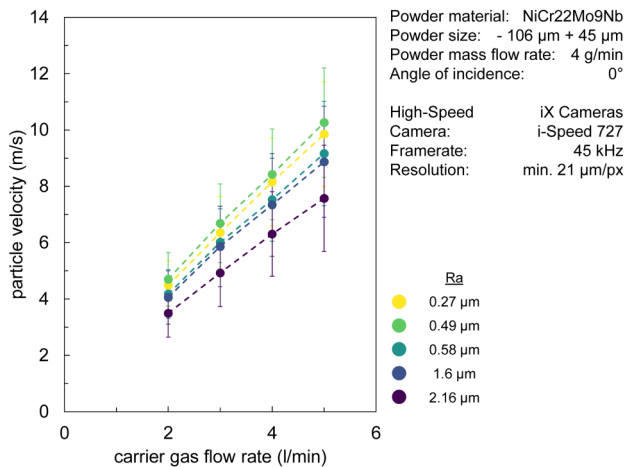


Bohlen 2024 BIAS ID 240237

FIG. 10. Divergence angle as a function of the carrier gas flow rate for different inner channel roughness Ra.

rate, the particle velocity remains constant. The lowest velocities are observed for the highest Ra value channel. Conversely, the highest particle velocities are recorded for the second lowest Ra value powder channel.

Figure 9 depicts the particle velocities for varying carrier gas flow rates across all inner channel roughnesses. It can be observed that an increase in carrier gas flow rate is accompanied by a seemingly linear increase in particle velocity for all channels. The powder channel with the highest Ra value exhibits the lowest particle velocities. The highest particle velocities are observed across all



Bohlen 2024 BIAS ID 240236

FIG. 9. Particle velocity as a function of the carrier gas flow rate for different inner channel roughness Ra.

carrier gas flow rates for the second lowest Ra value powder channel.

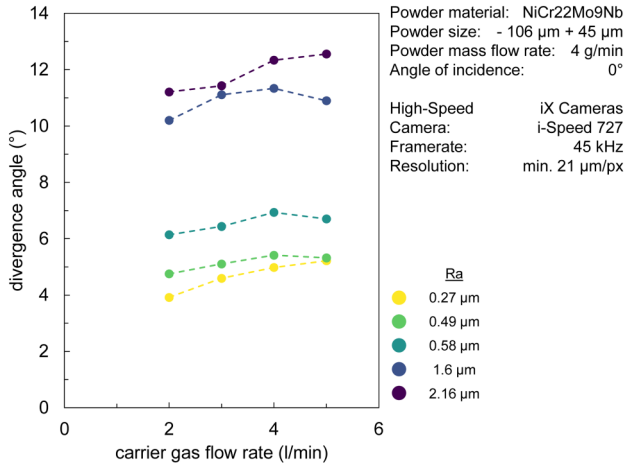
The divergence angle of the powder stream for different powder mass flow rates can be observed in Fig. 10. For the two roughest powder channels, the divergence angle appears to decrease with increasing powder mass flow rate. In contrast, the other three surface finishes exhibit a seemingly constant value with the increase in powder mass flow rate. The lowest values of divergence angle can be observed for the smoothest surface finish of Ra = 0.27 μm . The divergence angle values also increase in ascending order according to the Ra value.

With regard to the influence of inner channel roughness, similar observations could be made for an increasing carrier gas flow, as seen in Fig. 11. A slight increase in divergence angle can be observed for all inner channel roughnesses. Once again, the smoothest surface finish leads to the smallest divergence angles. Conversely, the highest surface roughness leads to the highest divergence angles.

The standard deviation of the surface roughness angle $\sigma\gamma$ was selected for $d_p > RSm$, as a greater proportion of the particles is larger than the respective RSm values. Figure 12 illustrates the particle velocity for varying carrier gas flow rates as a function of the angle $\sigma\gamma$. For each of the carrier gas flow rates, the particle velocities exhibit a slight decreasing trend with increasing angle $\sigma\gamma$. As the angle $\sigma\gamma$ increased from 0.42° to 2.17° (an increase of 423%), the mean particle velocity for a 2 l/min carrier gas flow rate decreased from 4.49 to 3.5 m/s (a decrease of 22%), while for a 5 l/min carrier gas flow rate, the mean particle velocity decreased from 9.85 to 7.57 m/s (a decrease of 23%).

Figure 13 depicts the divergence angle as a function of the surface roughness angle $\sigma\gamma$. An almost linear increase in the divergence angle can be observed as the angle $\sigma\gamma$ increases. The divergence angle does not exhibit significant differences for varying carrier gas flow rates. As the angle increases from 0.42° to 2.17° (an

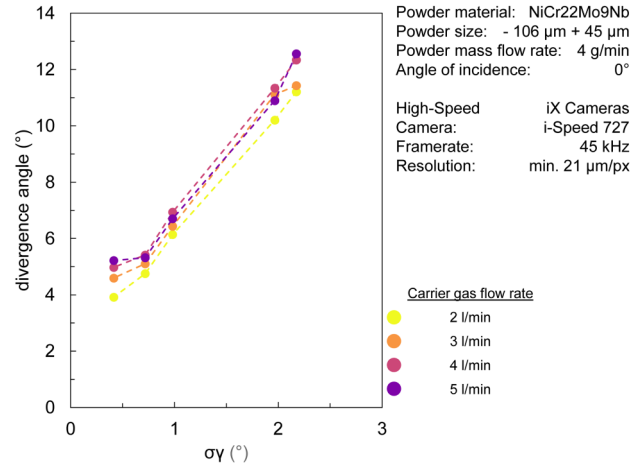
26 March 2025 14:09:59



Bohlen 2024

BIAS ID 240238

FIG. 11. Divergence angle as a function of the powder mass flow rate for different inner channel roughness Ra.



Bohlen 2024

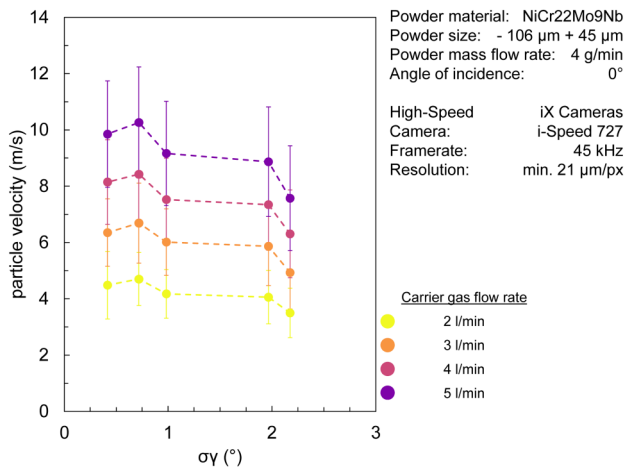
BIAS ID 240240

FIG. 13. Divergence angle as a function of the standard deviation of the surface roughness angle $\sigma\gamma$ for different carrier gas flow rates.

increase of 423%), the divergence angle increases by at least 140% for all carrier gas flow rates.

The velocity of the carrier gas demonstrates a nearly linear increase with an increase in the carrier gas flow rate (see Fig. 14). Additionally, the carrier gas velocity exhibits a slight decrease with an increase in inner wall roughness.

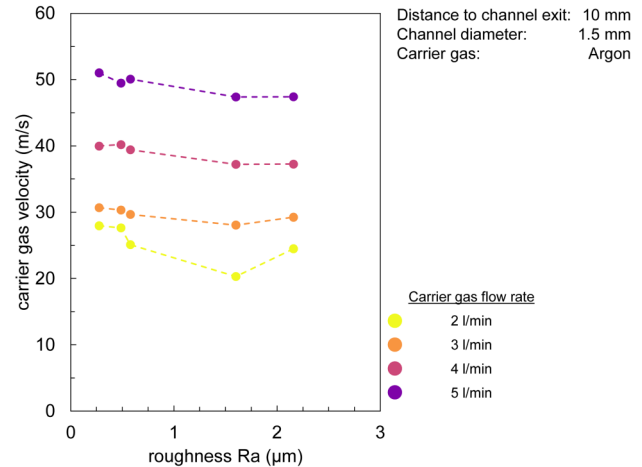
Figure 15 depicts the ratio between particle velocity and carrier gas velocity. For higher values of angle $\sigma\gamma$, a slight decrease in the ratio can be seen across all carrier gas flow rates.



Bohlen 2024

BIAS ID 240239

FIG. 12. Particle velocity as a function of the standard deviation of the surface roughness angle $\sigma\gamma$ for different carrier gas flow rates.

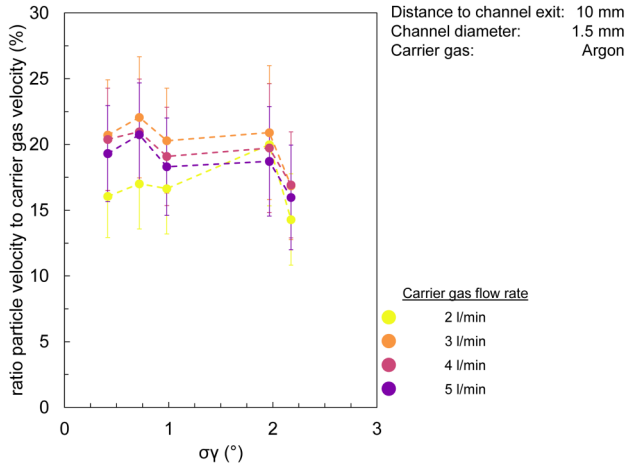


Bohlen 2024

BIAS ID 240241

FIG. 14. Carrier gas velocity as a function of roughness Ra of powder channels for different carrier gas flow rates.

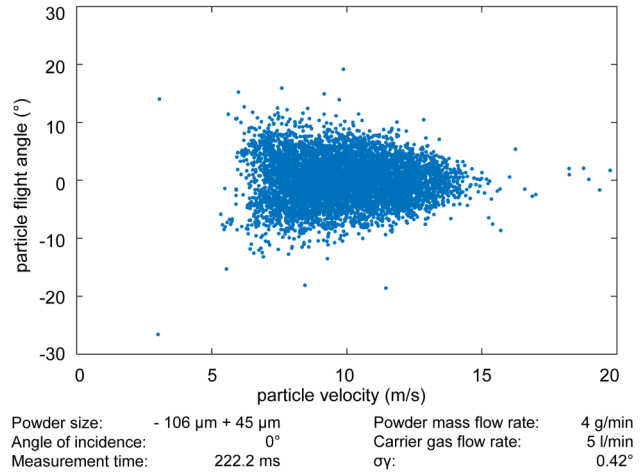
26 March 2025 14:09:59



Bohlen 2024

BIAS ID 240242

FIG. 15. Ratio of particle velocity to carrier gas velocity as a function of the standard deviation of the surface roughness angle $\sigma\gamma$ for different carrier gas flow rates.



Bohlen 2024

BIAS ID 240244

FIG. 17. Particle flight angles for tracked particles and their corresponding particle velocities for the low roughness channel (0.42°) with a high carrier gas flow rate (5 l/min).

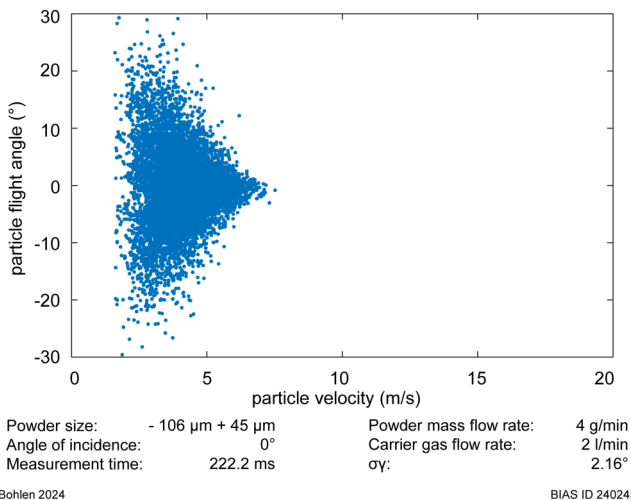
Figure 17 also represents a scatter plot for the particle velocities and their associated particle flight angles. In this measurement, compared to Fig. 16, the angle $\sigma\gamma$ decreased and the carrier gas flow rate increased. A shift of the particle velocities to higher velocities is observed. The lowest particle velocities start at approximately 6 m/s and spread up to 14 m/s. Once again, a symmetrical distribution of particle flight angle around 0° is evident. The distribution of angles is less distinct in this instance.

In order to facilitate comparison, only the two sigma values for the particle flight angle are plotted in Fig. 18. It is evident that for both angles $\sigma\gamma$ fast particles have a smaller flight angle. Increasing the carrier gas flow rate leads to a shift toward higher particle velocities, but does not change the distribution itself.

IV. DISCUSSION

The particle velocity is influenced by more than one parameter. For the carrier gas flow rate, an almost linear correlation to the

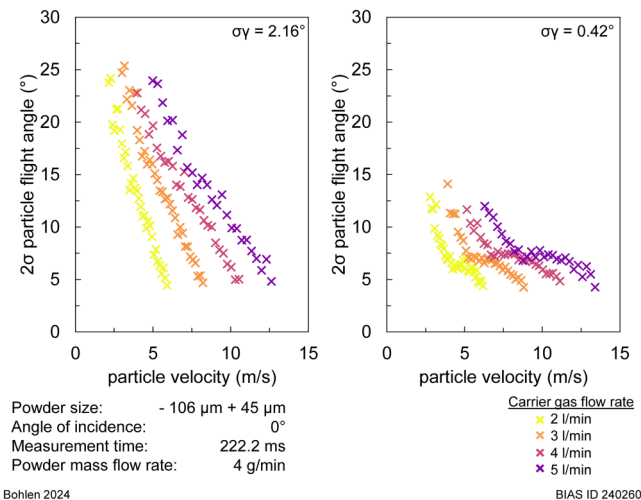
26 March 2025 14:09:59



Bohlen 2024

BIAS ID 240243

FIG. 16. Particle flight angles for tracked particles and their corresponding particle velocities for the high roughness channel (2.17°) with a low carrier gas flow rate (2 l/min).



Bohlen 2024

BIAS ID 240260

FIG. 18. Two sigma standard deviation of the particle flight angle as a function of the particle velocity for different angles $\sigma\gamma$ and carrier gas flow rates.

particle velocity can be seen (Fig. 9). In the case of a static powder channel inner diameter, an increase in carrier gas flow rate leads to a higher carrier gas velocity (Fig. 14), thus increasing the acceleration of powder particles. In addition to the carrier gas velocity, the angle $\sigma\gamma$ also influences the velocity of the powder particles. A decrease in Ra (and thus the standard deviation of the surface roughness angle $\sigma\gamma$) leads to a small increase in particle velocity (Fig. 12). A reduction in the standard deviation of the angle at which particles rebound from the inner powder channel wall will lead to a more direct particle trajectory through the powder channel. Consequently, particles traversing smoother powder channels are likely to experience a smaller number of particle-wall collisions, resulting in a diminished loss of kinetic energy and an augmented period for the carrier gas to accelerate the particles in between collisions. This is supported by the decrease in the ratio between particle velocity and carrier gas velocity with increasing angle $\sigma\gamma$ (Fig. 15).

The particle velocity is not influenced by the powder mass flow rate (Fig. 8). For the powder mass flow rates utilized in this study, particles contribute only a small amount to the total mass of the gas-particle stream. This limits the particle-particle interaction, thus minimizing the effect of powder mass flow rate on the particle velocity. A reduction in the angle $\sigma\gamma$ from 2.16° to 0.42° results in a reduction in carrier gas consumption while maintaining the same particle velocity distribution.

The divergence angle of the powder stream is primarily influenced by the inner surface roughnesses of the powder channels. The divergence angle increases almost linearly with the increase in $\sigma\gamma$ and is the same across different carrier gas flow rates (Fig. 13). This leads to the conclusion that the carrier gas flow rate does not have an influence on the divergence angle. The divergence angle is the result of the last collision of a particle inside the powder channel. As previously stated, a smaller angle $\sigma\gamma$ increases the probability of a particle having a more direct trajectory.

Figures 16 and 17 demonstrate that particles exhibiting a high velocity relative to the other particles in the experiment are more likely to display a straight trajectory (flight angle $\sim 0^\circ$) with respect to the powder channel. It is postulated that the last collision for these particles occurred further upstream, thereby allowing the carrier gas to accelerate the particles to a greater extent. Conversely, it is postulated that particles exhibiting a high flight angle can only achieve this if a collision with the powder channel occurs just before exiting the powder channel. Figure 18 illustrates that a smaller angle $\sigma\gamma$ leads to an overall smaller deviation in the particle flight angle. This phenomenon can be attributed to the assumption that particles within a powder channel with a low angle $\sigma\gamma$ exhibit straighter trajectories, resulting in a greater proportion of particles exiting the powder channel with a flight angle approaching 0° .

V. CONCLUSION

The impact of the inner surface roughness of powder channels on the divergence angle of the powder stream and the velocity and flight angle of individual particles was investigated.

- The parameter of the standard deviation of the surface roughness angle $\sigma\gamma$ provides a theoretical insight into the possible particle trajectories within a powder channel.

- The divergence angle of the powder stream is primarily determined by the angle $\sigma\gamma$. A reduction in the angle $\sigma\gamma$ from 2.16° to 0.42° (81%) resulted in a mean reduction in divergence angle of 61%. For a specific desired powder spot size, this implies an increase in working distance, thereby enhancing the robustness of the powder nozzle against process emissions and back reflection.
- The particle velocity is influenced by the angle $\sigma\gamma$. With smoother inner powder channels if a specific particle velocity is required, a lower carrier gas flow rate can be used to achieve this. This results in a potential reduction in process costs.

ACKNOWLEDGMENTS

The authors gratefully acknowledge the collaboration with the project partners Nutech GmbH, Schmelzmetall Deutschland GmbH, and Technische Universität Berlin regarding the support of knowledge, material, and equipment over the course of the research.

ZIM-Project No. KK5274710EW2 was funded by the Federal Ministry for Economic Affairs and Climate Action (BMWK) via the German Federation of Industrial Research Associations (AiF) in accordance with the policy to support the Central Innovations of Medium-Sized Enterprises (ZIM) based on a decision by the German Bundestag.

LUNOVU 835 LMD-Machine is funded by the Deutsche Forschungsgemeinschaft (DFG, German Research Foundation) under Project No. 434424600 (Highly flexible material synthesis and microstructure adjustment through combined laser deposition welding and short-term heat treatment for high-throughput materials development).

AUTHOR DECLARATIONS

Conflict of Interest

The authors have no conflicts to disclose.

Author Contributions

Annika Bohlen: Data curation (equal); Investigation (equal); Methodology (equal); Writing – original draft (lead). **Thomas Seefeld:** Funding acquisition (equal); Project administration (equal); Writing – review & editing (lead).

REFERENCES

- ¹M. Schmidt, M. Merklein, D. Bourell, D. Dimitrov, T. Hausotte, K. Wegener, L. Overmeyer, F. Vollertsen, and G. N. Levy, "Laser based additive manufacturing in industry and academia," *CIRP Ann.* **66**, 561–583 (2017).
- ²L. Li, Y. Huang, C. Zou, and W. Tao, "Numerical study on powder stream characteristics of coaxial laser metal deposition nozzle," *Crystals* **11**, 282 (2021).
- ³K. Odum, M. Soshi, and K. Yamazaki, "Measurement and analysis of impact dynamics suitable for modelling pneumatic transport of metallic powder flow through a directed energy deposition nozzle," *Adv. Powder Technol.* **33**, 103515 (2022).
- ⁴T. A. Polyanskiy, A. V. Zaitsev, I. P. Gulyaev, and A. M. Gurin, "Numerical and experimental investigation of two phase flow for direct metal deposition," *J. Phys.: Conf. Ser.* **1109**, 12010 (2018).
- ⁵A. Jeromen, A. Vidergar, M. Fujishima, G. N. Levy, and E. Govekar, "Powder particle-wall collision-based design of the discrete axial nozzle-exit shape in direct laser deposition," *J. Mater. Process. Technol.* **308**, 117704 (2022).

⁶M. Sommerfeld, “Modelling of particle-wall collisions in confined Gas-particle flows,” *Int. J. Multiphase Flow* **18**, 905–926 (1992).

⁷M. Sommerfeld and N. Huber, “Experimental analysis and modelling of particle-wall collisions,” *Int. J. Multiphase Flow* **25**, 1457–1489 (1999).

⁸G. A. Novelletto Ricardo and M. Sommerfeld, “Experimental evaluation of surface roughness variation of ductile materials due to solid particle erosion,” *Adv. Powder Technol.* **31**, 3790–3816 (2020).

⁹A. Haghshenas, A. Bohlen, D. Tyralla, and R. Groll, “The relevance of wall roughness modeling for simulation of powder flows in laser metal deposition nozzles,” *Int. J. Adv. Manuf. Technol.* **123**, 1441–1458 (2022).

¹⁰J.-Y. Tinevez, N. Perry, J. Schindelin, G. M. Hoopes, G. D. Reynolds, E. Laplantine, S. Y. Bednarek, S. L. Shorte, and K. W. Eliceiri, “Trackmate: An open and extensible platform for single-particle tracking,” *Methods (San Diego, Calif.)* **115**, 80–90 (2017).